Ultra-high liquid–solid thermal resistance using nanostructured gold surfaces coated with graphene

Cecilia Herrero, Laurent Joly, Samy Merabia

Ultra-high liquid-solid thermal resistance using nanostructured gold surfaces coated with graphene

Article *in* Applied Physics Letters · April 2022

DOI: 10.1063/5.0085944

3 authors:

Cecilia Herrero
Université de Montpellier
16 PUBLICATIONS **51** CITATIONS
SEE PROFILE

Laurent Joly
Claude Bernard University Lyon 1
105 PUBLICATIONS **3,921** CITATIONS
SEE PROFILE

Samy Merabia
French National Centre for Scientific Research
113 PUBLICATIONS **2,514** CITATIONS
SEE PROFILE

Ultra-high liquid-solid thermal resistance using nanostructured gold surfaces coated with graphene

Cecilia Herrero,[1] Laurent Joly,[1,2] and Samy Merabia[1,a)]
[1)] *Univ Lyon, Univ Claude Bernard Lyon 1, CNRS, Institut Lumière Matière, F-69622, VILLEURBANNE, France*
[2)] *Institut Universitaire de France (IUF), 1 rue Descartes, 75005 Paris, France*

(Dated: 6 April 2022)

The search for materials with high thermal resistance has promising applications in thermoelectric devices and boiling crisis retardation. In this paper, we study the interfacial heat transfer between water and gold, nanostructuring the gold surface and coating it with graphene. By trapping air (or vacuum in our simulations) between graphene and the nanopatterned surface, we observe a considerable increase in interfacial resistance compared to the planar gold situation, which is shown to scale with the effective graphene-gold contact surface for both monolayer and multilayer graphene. With the massive thermal resistances we predict (up to 200 nm in terms of Kapitza length), the system proposed here represents a robust alternative to superhydrophobic Cassie materials. Moreover, since the low thermal conductance is achieved primarily due to geometry (vacuum trapping), it is straightforward to extend our results to any material with a structure equivalent to that of the nanopatterned gold wall we considered here.

Modern computers are experiencing increasing levels of heating due to the quest of high operating frequencies. The maximal working temperatures are limited by the boiling crisis occurring when the liquid suddenly vaporizes, leading to solid components melting and degradation. Delaying the boiling crisis may be achieved through an increase of the solid-liquid interfacial thermal resistance – also named Kapitza resistance R, hence shifting the temperature at which explosive boiling occurs[1–4].

With that regard, there has been a growing interest in understanding the microscopic parameters that control R at liquid-solid interfaces. Documented parameters include wetting[5,6], roughness[7–10] and interfacial vibrational coupling[11,12]. These effects have been extensively characterized either experimentally[13–16], through molecular dynamics (MD) simulations[2,6–8,10–12,17–21], or analytically[22,23]. Another strategy to tune the Kapitza resistance relies on the intercalation of a third body between the solid and the liquid. For instance, self-assembled monolayers generally enhance interfacial transport[24–26]. By contrast, graphene has been shown to reduce the interfacial conductance between a material and water by taking advantage of the high cross-plane thermal resistance of multilayer graphene[27–30].

Although much less explored, an alternative path to achieve high Kapitza resistance is the use of superhydrophobic surfaces which, in the case of Cassie (or fakir) state materials, present a high thermal resistance due to the air trapping between the liquid and the solid[7,10]. Such fakir states are, however, characteristic of very non-wetting surfaces, which can be obtained by special chemical treatments[1,31,32] or nanostructuration[33]. Importantly also, stability is a major problem of Cassie states, which are not very robust under variations of pressure or in the presence of flows in the channel.

a)Electronic mail: Authors to whom correspondance should be addressed: cecil.herr@gmail.com, samy.merabia@univ-lyon1.fr

In this paper, we propose to use a graphene sheet to cover the nanostructured surface of a solid (gold in our case) to trap vacuum at the graphene-solid interface – with expected equivalent results than air trapping due to the small probability of having an air molecule contained at the scale of the pores), and exploit their low thermal conductivity to achieve low interfacial conductance between water and gold. Such graphene coated nanopillars present an alternative that can be extended to a wide range of common materials, and graphene stability can be improved by adding an increased number of graphene layers.

Using MD simulations, we assess that the conductance between nanostructured graphene and gold is proportional to the contact surface fraction between graphene and gold, with a smaller conductance for thinner nanopillars. Consequently, we report a giant Kapitza length ($\ell_K \sim 200$ nm, proportional to the Kapitza resistance) for the smallest surface fraction, being two orders of magnitude larger than the one reported for water-planar gold interface both in simulations[17] and experiments[5] ($\ell_K \sim 6$ nm), and one order of magnitude larger than the largest reported values in previous simulations on carbon nanotubes and graphite ($\ell_K \sim 30$ nm and $\ell_K \sim 50$ nm respectively)[27,34]. We also extend our simulations and description to multi-layer graphene systems, with the objective of presenting graphite, cheaper and stiffer than graphene, as a viable alternative to obtain the large ℓ_K presented for the most favorable geometries. The giant thermal resistance we obtain presents promising applications in delaying the temperature at which the boiling crisis occurs, and shows an alternative route to efficiently control thermal dissipation in nanofluidic systems.

We performed MD simulations, using the LAMMPS package[35], of TIP4P/2005 water[36] confined between different solid walls, in order to determine the system configuration that better enhances interface thermal resistance. Carbon-carbon interactions were modelled with the LCBOP force-field[37], carbon-water interactions from

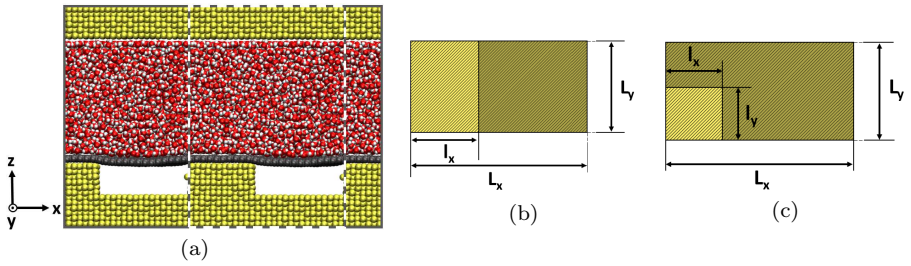

FIG. 1: Front view of the MD system for 1D and 2D structures. The original simulation box is represented in white dashed lines. (b) Top view of the 1D nanostructure where the surface fraction was varied by changing the l_x parameter. (c) Top view of the 2D nanostructure where the surface fraction was varied by changing l_x and l_y parameters.

Ref. 38 and carbon-gold interactions from Ref. 39. The gold-gold interactions were taken from Ref. 40, and the gold-water interactions from Ref. 41. The choice of the carbon-carbon potential is justified by its ability to reproduce the experimental phonon dispersion curves of graphene[42]. The Heinz potential has been chosen for gold-gold interactions as it gives a good account of gold elastic moduli and surface energy[40]. Last, the carbon-water and gold-water parameters work extremely well to recover experimental results for interfacial heat transfer for the water-gold interface[5], and are also in agreement with previous simulations with different interaction parameters[17] – see the supporting information (SI).

We tested the parameters for a water-planar gold configuration, obtaining good agreement with previous work, determining a Kapitza length $\ell_{\rm K}$ on the order of 8 nm (see the SI), and performed different tests by running MD simulations of a finite graphene sheet, supported on different gold nano-structures, in order to assess the stability of the suspended state and to make the pillar separation as large as possible while limiting graphene bending. We determined that graphene did not bend for pillars higher than 3 lattice parameters in the z direction (see the SI). After such stability had been assessed, we imposed periodic boundary conditions for the graphene sheet in the $x-y$ directions parallel to the walls. The system configuration, shown in Fig. 1a, consists in water enclosed between a graphene layer over a nano-structured gold surface at the bottom, and planar gold at the top. Due to the periodic boundary conditions, in order to suspend the graphene layer on the gold wall, we modified the crystallographic structure of the gold walls, thus corresponding to a modified FCC crystal with lattice parameters $\{a_x, a_y, a_z\} = \{4.216, 4.260, 4.173\}$ Å, with an imposed pillar height of $3a_z$. Note that equivalent results were obtained for the planar wall with the original and modified FCC lattices, and when considering taller pillars; see the SI. Two different nano-structures were studied. First, we explored the effect of 1D structures (Fig. 1b) for two different box sizes: $(L_x, L_y) = (14a_x, 14a_y)$ enclosing 5120 water molecules, and $(L_x, L_y) = (28a_x, 14a_y)$ enclosing 10240 water molecules. The pillar width l_x was varied between $3a_x$ and $20a_x$ in these simulations. Second, we explored the effect of 2D structures (Fig. 1c), where the system consisted in 10240 water molecules in a box size of lateral dimensions $(L_x, L_y) = (28a_x, 28a_y)$. The pillar area was imposed such as $l_x = ma_x$ and $l_y = ma_y$, with m varied between 6 and 9.

With regard to the simulation details, the Lennard-Jones interactions were truncated at $r_{\rm cutoff} = 12$ Å, and the equations of motion were integrated using the velocity-Verlet algorithm with a simulation timestep of 1 fs. In all the simulations, we first performed an equilibration run of 0.9 ns where we settled the pressure to 1 atm, using the top wall as a piston, so that the distance between the two innermost solid layers was $H \sim 38$ Å, with a well defined bulk region in the middle of the channel. During the first 0.3 ns of such equilibration we applied a Nosé-Hoover thermostat to the fluid atoms while keeping the carbon atoms frozen during the first 0.2 ns; next, both fluid and carbon atoms were thermostated at $T = 300$ K. The fluid and carbon atoms were not thermostated during the production run, of 0.5 ns. In both simulation steps we applied a Nosé-Hoover thermostat to all the wall atoms except the ones in the outermost layers which were frozen. The top and bottom walls were thermalized at $T \pm {\rm d}T/2$ respectively, with $T = 300$ K and ${\rm d}T = \{40, 60, 80\}$ K, which corresponded to the linear response regime as we verified, by checking that equivalent results of the thermal transport coefficients were obtained for the three values of ${\rm d}T$. Note that all the simulation procedure was analogous for the multilayered graphene simulations. More details on the simulation procedure can be found in the SI.

The main objective of nanopatterning the gold surface is to reduce the conductance $G = 1/R$ (*i.e.* to increase the resistance R) between water and gold by maintaining a fakir state between water and the gold walls exploiting the low thermal conductivity of vacuum. With this

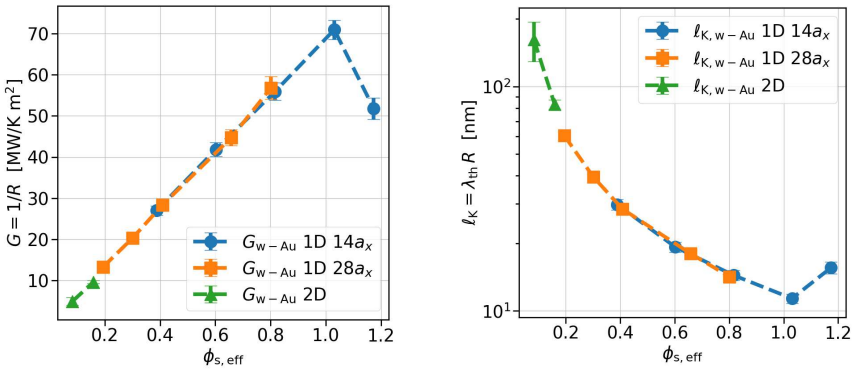

FIG. 2: Total water-gold (a) conductance G and (b) Kapitza length ℓ_{K} scaling with the effective graphene-gold contact surface area $\phi_{\mathrm{s,eff}}$. The different symbols correspond to the simulation results and dashed lines connect the symbols.

regard, we observed a decrease of the water-gold conductance $G_{\mathrm{w-Au}}$, with the decrease of the graphene-gold contact surface fraction $\phi_{\mathrm{s}} = l_x l_y/(L_x L_y)$ by one order of magnitude of difference between the planar gold situation and the configuration with the smallest ϕ_{s}, (see Fig. 2a and the SI). Therein, we propose a simple model in order to describe these results.

We start from the continuity condition of the temperature jumps at the water-carbon-gold interfaces, *i.e.* $\Delta T_{\mathrm{w-Au}} = \Delta T_{\mathrm{w-C}} + \Delta T_{\mathrm{C-Au}}$ (with $\Delta T_{\mathrm{A-B}} = T_{\mathrm{B}} - T_{\mathrm{A}}$). Taking into account that the thermal resistance is given by $R = \Delta T/j_{\mathrm{h}}$ with the heat flux j_{h} being constant in the whole channel, it is then a necessary condition that the water-carbon and carbon-gold interfaces act as a pair of resistances connected in series, so for the planar gold wall $R_{\mathrm{w-Au}} = R_{\mathrm{w-C}} + R_{\mathrm{C-Au}}$. We can introduce the effect of the contact surface fraction by supposing that it will modify the carbon-gold thermal resistance as $R_{\mathrm{w-Au}}/\phi_{\mathrm{s,eff}}$, where $\phi_{\mathrm{s,eff}}$ refers to an effective surface fraction. Such effective $\phi_{\mathrm{s,eff}}$ accounts for the extension of the graphene-gold surface of contact over a small distance r_{c}, related to the effective extension of the carbon-gold atomic interactions. In this way,

$$R_{\mathrm{w-Au}} = R_{\mathrm{w-C}} + \frac{R_{\mathrm{C-Au}}}{\phi_{\mathrm{s,eff}}}, \tag{1}$$

where $\phi_{\mathrm{s,eff}}$ is given, for a 1D structure,by:

$$\phi_{\mathrm{s,eff}} = \frac{l_x + 2r_{\mathrm{c}}}{L_x};$$

and for a 2D structure, by:

$$\phi_{\mathrm{s,eff}} = \frac{(l_x + 2r_{\mathrm{c}})(l_y + 2r_{\mathrm{c}}) - 4r_{\mathrm{c}}^2}{L_x L_y};$$

where we subtracted a $4r_{\mathrm{c}}^2$ area to not overestimate the real effect of r_{c} by just considering the rectangle area given by $(l_x + 2r_{\mathrm{c}})(l_y + 2r_{\mathrm{c}})$.

We fitted with Eq. (1) the $R_{\mathrm{w-Au}}$ results obtained from a variety of geometrical configurations (see the SI). The resulting resistances are $R_{\mathrm{w-C}} = 3.84 \times 10^{-10} \pm 7.67 \times 10^{-10}$ K·m^2/W, $R_{\mathrm{C-Au}} = 1.42 \times 10^{-8} \pm 9.47 \times 10^{-10}$ K·m^2/W (in agreement with the measured value for the planar gold surface) and $r_{\mathrm{c}} = 5.12 \pm 0.54$ Å. Although the error bars in the fitted water-carbon resistance are large, we can assess the quality of the fit by plotting the measured $G_{\mathrm{w-Au}}$ as a function of the effective surface fraction $\phi_{\mathrm{s,eff}}$. The results for all the 1D and 2D structures are plotted in Fig. 2a. One can see that all the results collapse on the same curve with $r_{\mathrm{c}} = 5.12$ Å (so $r_{\mathrm{c}} \sim 0.4\, r_{\mathrm{cutoff}}$), verifying the $G_{\mathrm{w-Au}}$ scaling with the effective surface fraction for all the different geometries considered. In Fig. 2a one also observes a deviation from the linear behavior for the point having $\phi_{\mathrm{s}} = 1$ ($\phi_{\mathrm{s,eff}} \sim 1.2$), corresponding to the planar gold wall case. Our interpretation is the following: the effective surface fraction $\phi_{\mathrm{s}} = 1$ leads to maximum thermal conductance as a result of both the relative large contact surface fraction between gold and water and of the possible bending of the graphene layers in the $\sim$ 1-nm spacing between neighbor pillars. Indeed, bending modes carry most of the heat in graphene as shown in Ref. 43. In the planar gold wall system, these bending modes are frozen, hence the graphene in-plane conductivity decreases, explaining the decreased interfacial conductance. Further work should be carried out to understand the conductance decrease for this geometry with respect to the nanopatterned surface.

It is interesting to quantify the contribution of the graphene coated nanopillars in the increase of the ther-

mal resistance in terms of the Kapitza length $\ell_K = \lambda_{th}/G$, with λ_{th} the thermal conductivity of water at 300 K, taken as $\lambda_{th} = 0.8$ W/(K·m), see the SI. We see in Fig. 2b that the Kapitza lengths measured in our system range from 10 to 200 nm, and Eq. (1) predicts even a higher ℓ_K by lowering the effective surface fraction. We would like to highlight the high ℓ_K values obtained for our supported graphene simulations for the smallest $\phi_{s,eff}$. These values are significantly higher than the exceptional values obtained for more complex structures, such as CNT with $\ell_K \sim 30$ nm for the most confined system[34] or $\ell_K \sim 50$ nm for graphite supported on planar copper[27]. Therefore, nanostructured graphene coated systems are promising to realize interfaces with ultra high Kapitza resistance.

To go further, the presented results could be extended by adding graphene layers between water and the gold nanopillars, with graphite being a cheaper and stiffer material than graphene, and for which, based on the results of Ref. 27 for water-planar copper, one could expect even higher resistance. With this regard, we performed MD simulations for different numbers of graphene layers (N from 1 to 5; a system snapshot of the planar gold geometry with $N = 5$ is represented in Fig. 3a). In Fig. 3b the water-gold thermal conductance is represented for different geometries. One can see in this figure that, for the higher surface fraction of $\phi_s = 1$, adding graphene layers has a large effect on the measured G as compared with the $N = 1$ situation, although for $N > 2$ the impact on G is very small. However, for the geometries characterized by smaller ϕ_s, one can observe a minimal impact of considering multilayered graphene walls.

One can understand these results within the proposed model. Defining the graphene layer closer to the gold wall C_1 and $\{C_2, ..., C_N\}$ the successive layers (see Fig. 3a), Eq. (1) can be extended as:

$$R_{w-Au} = R_{w-C_N} + \sum_{i>1}^{N-1} R_{C_{i+1}-C_i} + R_{C_2-C_1} + \frac{R_{C_1-Au}}{\phi_{s,eff}}. \quad (2)$$

In Fig. 3a, showing the temperature profile of the different components of the system, one can see that, since $R \propto \Delta T$, the main resistances that contribute to the water-gold resistance are R_{Au-C_1} and $R_{C_1-C_2}$, yielding a simplified Eq. (2):

$$R_{w-Au} \simeq R_{C_2-C_1} + \frac{R_{C_1-Au}}{\phi_{s,eff}}. \quad (3)$$

This expression allows us to understand the results presented on Fig. 3b. When $\phi_{s,eff} \ll 1$, then $R_{C_1-Au}/\phi_{s,eff} \gg R_{C_2-C_1}$, implying a very small effect of adding graphene layers as compared to the monolayer situation. Nevertheless, when $\phi_{s,eff}$ is on the order of one, then $R_{C_1-Au}/\phi_{s,eff} \sim R_{C_2-C_1}$, having a strong impact in the resistance of adding a graphene layer (around a factor of 2) and, thus, on its inverse G. Still, in these large $\phi_{s,eff}$ situations the following temperature jumps between C_i and C_{i+1} for $i > 1$ in Eq. (2) are still very small as compared to the gold-C_1 and C_1-C_2 temperature jumps, and the effect of adding more graphene layers for $N > 2$ is very small even for these systems. The concentration of the temperature jump at the C_1-C_2 interface may be qualitatively explained by the fact that already the second layer does not interact with gold and should see a bulk-like environment. By contrast, the vibrational properties of the first layer are strongly affected by the presence of gold, which results in a mismatch with the vibrational properties of C_2 and a more pronounced temperature jump. Finally, one can see in Fig. 3a that the temperature gradient across the carbon monolayers (apart of the first one C_1) is comparable to the temperature gradient across water. This similarity can be understood in terms of the similar thermal conductivities of water[44,45] and graphite[46], both on the order of $\lambda_{th} \sim 0.7$ W/(K·m).

In conclusion, we explored via non-equilibrium molecular dynamics simulations the effect on gold-water interfacial heat transfer of nanopatterning the solid wall and covering it with a graphene sheet. In the case of planar gold walls, we observed that the Kapitza length increased by a factor of ~ 2.5 by adding a graphene layer at the gold-water interface, in agreement with previous results obtained for the copper-graphene-water interface[27]. For nanopatterned walls, first, we observed that graphene did not bend around the wall nanopillars for heights larger than ~ 12.5 Å, independently of the pillar separation, thus trapping vacuum (equivalent to air trapping at the scale of the pores) between the gold and the graphene layer. We then showed that this vacuum trapping resulted in an increase of the interfacial Kapitza resistance R. We observed very good agreement of our results with the model, with a perfect linear dependency of the thermal conductance $G = 1/R$ with the effective surface fraction. Very high Kapitza lengths were observed for the smaller surface fraction systems, with a maximum of $\ell_K \sim 200$ nm, much higher as compared to previous values obtained for CNT ($\ell_K \sim 30$ nm[34]) or graphite-planar copper ($\ell_K \sim 50$ nm[27]) interfaces; the model predicts that even larger ℓ_K can be obtained by reducing further the surface fraction. These values were recovered for a multilayer graphene system in a similar geometry, pointing to graphite as a viable alternative, cheaper and stiffer than graphene, and thus improving the system stability.

These results pave the way to the design of nanomaterials to control heat dissipation. Particularly, the coated structure hold some promise for applications where a high Kapitza resistance is needed. The proposed system presents a cheap and robust alternative to superhydrophobic surfaces – where the Kapitza resistance is increased for so-called "Cassie materials" for which air is trapped below the liquid drop due to the liquid-solid wetting properties[31,32] – extendable to any type of material having a structure comparable to the nanopatterned

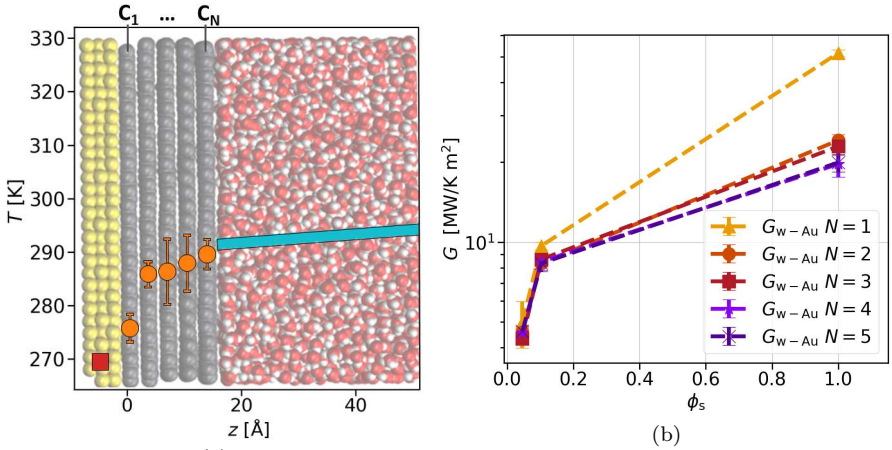

FIG. 3: (a) MD simulation snapshot of the planar gold wall configuration coated with $N = 5$ graphene layers. The temperature profile across the system components is also represented. The temperature points are averaged over three independent configurations. For reference we plot the theoretical temperature profile of water. (b) Total water-gold conductance as a function of the surface fraction ϕ_s for different number N of graphene layers.

gold wall.

SUPPLEMENTARY MATERIAL

The supplementary material contains details on the construction of the systems, on the interatomic potentials and on the thermal transfer measurements.

ACKNOWLEDGMENTS

The authors thank C. Barentin, G. Galliero and C. Leonard for interesting discussions. We are also grateful for HPC resources from GENCI/TGCC (grants A0070810637 and A0090810637), and from the PSMN mesocenter in Lyon. LJ is supported by the Institut Universitaire de France.

[1] I. U. Vakarelski, N. A. Patankar, J. O. Marston, D. Y. Chan, and S. T. Thoroddsen, "Stabilization of Leidenfrost vapour layer by textured superhydrophobic surfaces," Nature **489**, 274–277 (2012).
[2] H. Han, S. Mérabia, and F. Müller-Plathe, "Thermal Transport at Solid-Liquid Interfaces: High Pressure Facilitates Heat Flow through Nonlocal Liquid Structuring," Journal of Physical Chemistry Letters **8**, 1946–1951 (2017).
[3] H. Han, S. Merabia, and F. Müller-Plathe, "Thermal transport at a solid-nanofluid interface: From increase of thermal resistance towards a shift of rapid boiling," Nanoscale **9**, 8314–8320 (2017).
[4] R. Liu and Z. Liu, "Rapid thermal transport at rough solid-fluid interface: Evaporation and explosive boiling on concave nanostructure," International Journal of Heat and Mass Transfer **154**, 119676 (2020).
[5] Z. Ge, D. G. Cahill, and P. V. Braun, "Thermal conductance of hydrophilic and hydrophobic interfaces," Physical Review Letters **96**, 1–4 (2006).
[6] L. Xue, P. Keblinski, S. R. Phillpot, S. U. Choi, and J. A. Eastman, "Two regimes of thermal resistance at a liquid-solid interface," Journal of Chemical Physics **118**, 337–339 (2003).
[7] Y. Wang and P. Keblinski, "Role of wetting and nanoscale roughness on thermal conductance at liquid-solid interface," Applied Physics Letters **99**, 2011–2014 (2011).
[8] Y. Chen and C. Zhang, "Role of surface roughness on thermal conductance at liquid-solid interfaces," International Journal of Heat and Mass Transfer **78**, 624–629 (2014).
[9] E. Lee, T. Zhang, T. Yoo, Z. Guo, and L. Tengfei, "Nanostructures signicantly enhance thermal transport across solid interfaces," ACS Applied Material Science **8**, 35505–35512 (2016).
[10] D. Surblys, Y. Kawagoe, M. Shibahara, and T. Ohara, "Molecular dynamics investigation of surface roughness scale effect on interfacial thermal conductance at solid-liquid interfaces," The Journal of chemical physics **150**, 114705 (2019).
[11] S. Ge and M. Chen, "Vibrational coupling and Kapitza resistance at a solid-liquid interface," International Journal of Thermophysics **34**, 64–77 (2013).
[12] K. Sääskilahti, J. Oksanen, J. Tulkki, and S. Volz, "Spectral mapping of heat transfer mechanisms at liquid-solid interfaces," Physical Review E **93**, 1–8 (2016), arXiv:1512.05914.
[13] J. Park, J. Huang, W. Wang, C. J. Murphy, and D. G. Cahill, "Heat transport between Au nanorods, surrounding liquids, and solid supports," Journal of Physical Chemistry C **116**, 26335–26341 (2012).
[14] T. Stoll, P. Maioli, A. Crut, S. Rodal-Cedeira, I. Pastoriza-Santos, F. Vallée, and N. Del Fatti, "Time-Resolved Investigations of the Cooling Dynamics of Metal Nanoparticles: Impact of Environment," The Journal of Physical Chemistry C **119**, 12757–12764 (2015).
[15] J. Park and D. G. Cahill, "Plasmonic Sensing of Heat Transport at Solid-Liquid Interfaces," Journal of Physical Chemistry C **120**, 2814–2821 (2016).

[16]J. A. Tomko, D. H. Olson, A. Giri, J. T. Gaskins, B. F. Donovan, S. M. O'Malley, and P. E. Hopkins, "Nanoscale wetting and energy transmission at solid/liquid interfaces," Langmuir **35**, 2106–2114 (2019).
[17]A. Pham, M. Barisik, and B. Kim, "Pressure dependence of Kapitza resistance at gold/water and silicon/water interfaces," Journal of Chemical Physics **139**, 244702 (2013).
[18]A. Giri and P. E. Hopkins, "Spectral analysis of thermal boundary conductance across solid/classical liquid interfaces: A molecular dynamics study," Applied Physics Letters **105**, 33106 (2014).
[19]V. R. Ardham and F. Leroy, "Communication: Is a coarse-grained model for water sufficient to compute Kapitza conductance on non-polar surfaces?" Journal of Chemical Physics **147**, 151102 (2017).
[20]S. Alosious, S. K. Kannam, S. P. Sathian, and B. D. Todd, "Kapitza resistance at water-graphene interfaces," The Journal of chemical physics **152**, 224703 (2020).
[21]M. Masuduzzaman and B. Kim, "Scale effects in nanoscale heat transfer for fourier's law in a dissimilar molecular interface," ACS omega **5**, 26527–26536 (2020).
[22]M. E. Caplan, A. Giri, and P. E. Hopkins, "Analytical model for the effects of wetting on thermal boundary conductance across solid/classical liquid interfaces," The Journal of Chemical Physics **140**, 154701 (2014).
[23]S. Merabia, J. Lombard, and A. Alkurdi, "Importance of viscoelastic and interface bonding effects in the thermal boundary conductance of solid-water interfaces," International Journal of Heat and Mass Transfer **100**, 287–294 (2016).
[24]G. Kikugawa, T. Ohara, T. Kawaguchi, I. Kinefuchi, and Y. Matsumoto, "A molecular dynamics study on heat transfer characteristics over the interface of self-assembled monolayer and water solvent," Journal of Heat Transfer **136**, 102401 (2014).
[25]Z. Tian, A. Marconnet, and G. Chen, "Enhancing solid-liquid interface thermal transport using self-assembled monolayers," Applied Physics Letters **106**, 1–5 (2015).
[26]T. Zhang, A. R. Gans-Forrest, E. Lee, X. Zhang, C. Qu, Y. Pang, F. Sun, and T. Luo, "Role of hydrogen bonds in thermal transport across hard/soft material interfaces," ACS Applied Material Science **8**, 33326–33334 (2016).
[27]A. T. Pham, M. Barisik, and B. H. Kim, "Interfacial thermal resistance between the graphene-coated copper and liquid water," International Journal of Heat and Mass Transfer **97**, 422–431 (2016).
[28]B. Y. Cao, J. H. Zou, G. J. Hu, and G. X. Cao, "Enhanced thermal transport across multilayer graphene and water by interlayer functionalization," Applied Physics Letters **112**, 1–5 (2018).
[29]C. U. Gonzalez-Valle, L. E. Paniagua-Guerra, and B. Ramos-Alvarado, "Implications of the Interface Modeling Approach on the Heat Transfer across Graphite-Water Interfaces," Journal of Physical Chemistry C **123**, 22311–22323 (2019).
[30]G. Chen, J. Chen, and Z. Wang, "Thermal Transport at Interface Between Single-Layer Graphene and Water Film," International Journal of Thermophysics **41**, 1–19 (2020).
[31]A. Lafuma and D. Quéré, "Superhydrophobic states," Nature Materials **2**, 457–460 (2003).
[32]D. Quéré, "Wetting and roughness," Annual Review of Materials Research **38**, 71–99 (2008).
[33]A. Giacomello, L. Schimmele, S. Dietrich, and M. Tasinkevych, "Recovering superhydrophobicity in nanoscale and macroscale surface textures," Soft Matter **15**, 7462–7471 (2019).
[34]S. Alosious, S. K. Kannam, S. P. Sathian, and B. D. Todd, "Nanoconfinement Effects on the Kapitza Resistance at Water-CNT Interfaces," Langmuir **37**, 2355–2361 (2021).
[35]A. P. Thompson, H. M. Aktulga, R. Berger, D. S. Bolintineanu, W. M. Brown, P. S. Crozier, P. J. in 't Veld, A. Kohlmeyer, S. G. Moore, T. D. Nguyen, R. Shan, M. J. Stevens, J. Tranchida, C. Trott, and S. J. Plimpton, "Lammps - a flexible simulation tool for particle-based materials modeling at the atomic, meso, and continuum scales," Computer Physics Communications **271**, 108171 (2022).
[36]J. L. Abascal and C. Vega, "A general purpose model for the condensed phases of water: TIP4P/2005," Journal of Chemical Physics **123**, 1–12 (2005).
[37]H. Los and A. Fasolino, "Intrinsic long-range bond-order potential for carbon: Performance in Monte Carlo simulations of graphitization," Physical Review B - Condensed Matter and Materials Physics **68**, 24107 (2003).
[38]K. Falk, F. Sedlmeier, L. Joly, R. R. Netz, and L. Bocquet, "Molecular Origin of Fast Water Transport in Carbon Nanotube Membranes: Superlubricity versus Curvature Dependent Friction," Nano Letters **10**, 4067–4073 (2010).
[39]M. Neek-Amal, R. Asgari, and M. R. Rahimi Tabar, "The formation of atomic nanoclusters on graphene sheets," Nanotechnology **20**, 135602 (2009), arXiv:0810.3385.
[40]H. Heinz, R. A. Vaia, B. L. Farmer, and R. R. Naik, "Accurate simulation of surfaces and interfaces of face-centered cubic metals using 12-6 and 9-6 lennard-jones potentials," Journal of Physical Chemistry C **112**, 17281–17290 (2008).
[41]S. Merabia, S. Shenogin, L. Joly, P. Keblinski, and J.-L. Barrat, "Heat transfer from nanoparticles: a corresponding state analysis." Proceedings of the National Academy of Sciences of the United States of America **106**, 15113–15118 (2009), arXiv:0906.0438.
[42]P. Rowe, G. Csányi, D. Alfè, and A. Michaelides, "Development of a machine learning potential for graphene," Physical Review B **97**, 54303 (2018), arXiv:1710.04187.
[43]D. B. L. Lindsay and N. Mingo, "Flexural phonons and thermal transport in graphene," Phys. Rev. B **82**, 115427 (2010).
[44]M. L. Ramires, C. A. Nieto Castro, Y. Nagasaka, A. Nagashima, M. J. Assael, and W. A. Wakeham, "Standard Reference Data for the Thermal Conductivity of Water," Journal of Physical and Chemical Reference Data **24**, 1377–1381 (1995).
[45]F. Römer, A. Lervik, and F. Bresme, "Nonequilibrium molecular dynamics simulations of the thermal conductivity of water: a systematic investigation of the SPC/E and TIP4P/2005 models." The Journal of Chemical Physics **137**, 74503 (2012).
[46]M. Harb, C. von Korff Schmising, H. Enquist, A. Jurgilaitis, I. Maximov, P. V. Shvets, A. N. Obraztsov, D. Khakhulin, M. Wulff, and J. Larsson, "The c-axis thermal conductivity of graphite film of nanometer thickness measured by time resolved x-ray diffraction," Applied Physics Letters **101**, 233108 (2012), https://doi.org/10.1063/1.4769214.

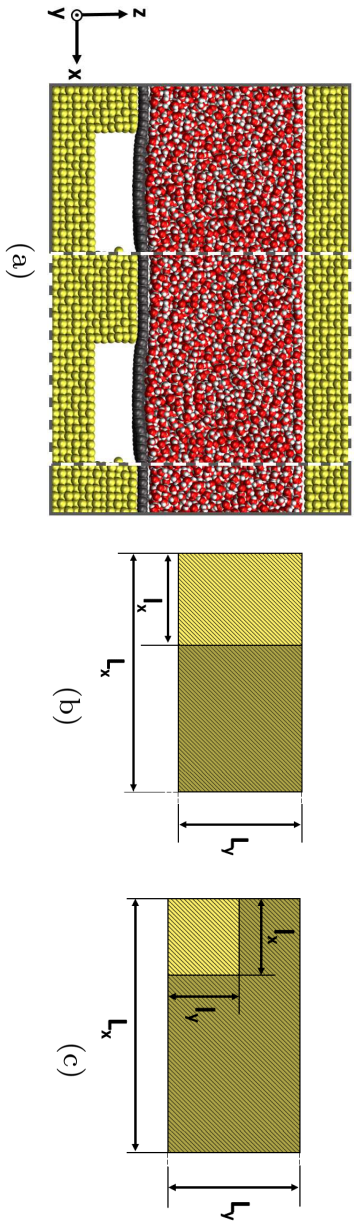

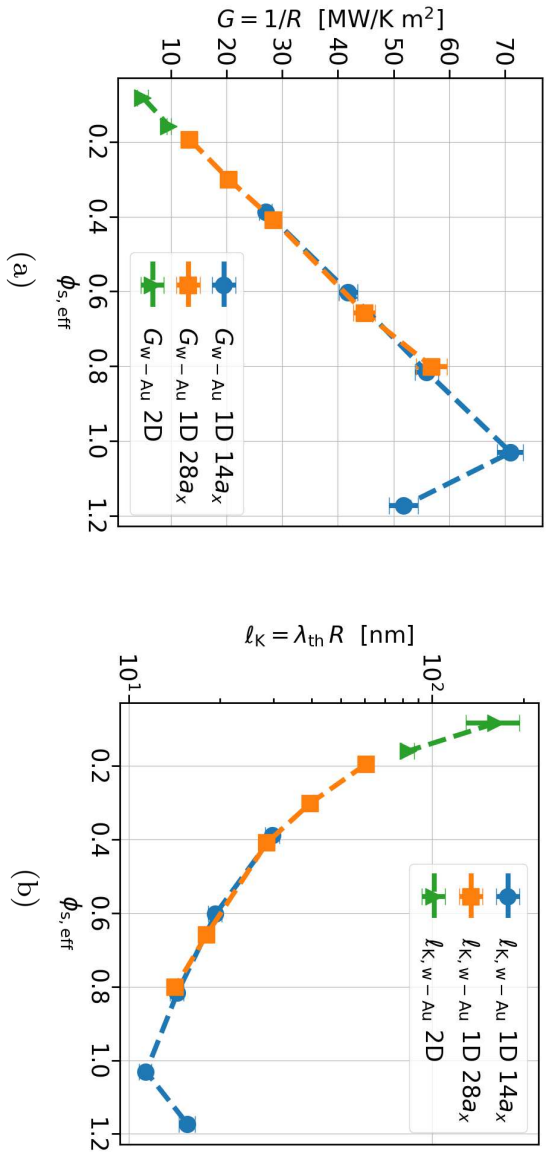

AIP Publishing

Applied Physics Letters ACCEPTED MANUSCRIPT

This is the author's peer reviewed, accepted manuscript. However, the online version of record will be different from this version once it has been copyedited and typeset.

PLEASE CITE THIS ARTICLE AS DOI: 10.1063/5.0085944